Date of publication xxxx 00, 0000, date of current version xxxx 00, 0000.

Digital Object Identifier 10.1109/ACCESS.2024.0429000

EMI Simulation of Permanent Magnet Motor Drive Systems

YERAI MORENO[1], GAIZKA ALMANDOZ[1] (Member, IEEE), ARITZ EGEA[1], IMANOL EGUREN[1] and ANDER URDANGARIN[2]

[1]Faculty of Engineering, Mondragon Unibertsitatea, 20500 Mondragón, Spain
[2]ORONA EIC, 20120 Hernani, Spain

Corresponding author: Yerai Moreno (e-mail: ymoreno@mondragon.edu).

The work of Yerai Moreno was funded by the Non-Doctoral Research Staff Training Programme of the Department of Education of the Basque Government through grant PRE-2023-2-0001.

ABSTRACT With increasing emphasis on energy efficiency and the widespread adoption of Wide-Band-Gap (WBG) devices, understanding and mitigating EMI is crucial for the reliability and performance of electric drives. This research focuses on high-frequency phenomena induced in electrical machines and the integration of Finite Element Method (FEM) simulations into the drive design process. A novel approach is introduced where a full drive model is experimentally validated using motor impedance obtained from FEM simulations, which is then fitted to a lumped-parameter model with a basic genetic algorithm. The model is validated across the full Electromagnetic Compatibility (EMC) range for conducted emissions, from 10 kHz to 30 MHz. The paper emphasises the importance of an EMI-focused design approach early in the development process to minimise costs, improve reliability, and ensure compliance with EMC standards.

INDEX TERMS Electric drive, electromagnetic interference, electric machine, high frequency.

I. INTRODUCTION

UNITED Nations' Sustainable Development Goals aim to end poverty, protect the planet, and ensure prosperity by 2030, with a focus on clean energy and climate action [1]. Meanwhile, the European Commission has established targets to enhance energy efficiency across various sectors, emphasising the adoption of energy-efficient technologies [2].

It is estimated that electrical drives account for over 40% of global electricity consumption, thereby highlighting their critical role in sustainability efforts [3]. Recent studies have identified the potential of Wide-Band-Gap (WBG) devices, such as those made of Silicon Carbide (SiC), to significantly improve drive performance. These devices enhance power density, dynamic response end thermal conductivity enabling the design of more efficient and compact inverter and motor configurations [4], [5].

However, using WBG devices at elevated frequencies can lead to Electromagnetic Interference (EMI) due to increased voltage derivatives. This can compromise the durability of electrical machines and other electronic devices, potentially leading to malfunctions. Converters provide electrical machines with voltages modulated in frequency and amplitude, which are capable of producing significant voltage derivatives. As frequencies rise, voltage derivatives escalate, causing overvoltages at motor terminals and potentially deteriorating the insulation of the windings and protection mechanisms during short circuits or contact anomalies [5]–[7].

Another concern is Common Mode Voltage (CMV) generated by modulated voltages, which can damage drive components and impact other devices on the same network. For instance, voltage in the shaft may induce bearing currents, resulting in their degradation [8].

To address these challenges, strategies have been proposed to mitigate unwanted CMV on shafts and bearings. These include using insulated or ceramic bearings, applying conductive greases, and incorporating Faraday shielding or shaft grounding rings [9], [10]. However, these methods primarily focus on bearing-related consequences.

For broader EMI reduction in electrical machines, it is recommended to use shielded cables combined with grounding to establish a low-impedance path for CMV. In addition, several inverter designs and modulation strategies have been proposed to minimise CMV production at the source [5], [9], [11]–[13].

Typically, incorporating filters into drive systems is actually the most common way to reduce EMI, which not only raises its cost, size, and weight, but also adds to the system's complexity [14]. Moreover, they are generally added only after failing Electromagnetic Compatibility (EMC) tests, necessitating corrective measures to meet regulatory standards and market the product. Consequently, it is advisable to incorporate an EMI-focused design approach early in the development process to minimise costs, enhance reliability, reduce time to market, and secure the best possible outcome, effectively managing EMI noise at the device level.

Despite the interest in high-frequency simulations of electrical drives for EMI analysis or other issues, few studies have considered these models for the design stage. In fact, most articles are based on behavioural models obtained from experimentally measured impedances of the motor, making them unsuitable for the design stage, since an already manufactured motor is needed [15]–[21].

Furthermore, most of them are only valid up to 10 MHz, which is not enough for the full EMC range established by the regulations [22].

In addition, few studies have analysed the machine with Finite Element Method (FEM) simulations to integrate it into the complete drive model [23]. However, the common-mode current spectrum is only validated up to 1.8 MHz.

To fill the gap in the EMI simulations on electric drives for the design stage, the following contributions are contained in this paper:

- A full drive model is presented and experimentally validated using a Si-IGBT converter. The model uses the motor impedance obtained from FEM simulations, validated with measurements of a set of 28 units of an industrial electrical machine, making it suitable for the drive design stage.
- The validity of this model in the full EMC range for conducted emissions is demonstrated, as very good agreement with the experimental results is obtained in the range of 150 kHz-30 MHz.
- The filter used for the compliance with the EMC standard is also modelled and validated within the model. This makes the model suitable for sizing the filter for each specific application to meet EMC regulations.

This is a continuation of previous works. In [24] the state of the art is systematically reviewed, analysing different high-frequency phenomena induced in electrical machines, together with the tools used to address these phenomena. Then, in [25], a high accuracy and low computational load simulation approach is presented to calculate the high frequency impedance of electrical machines. The model is validated with the impedance measurement of 28 industrial motors.

The structure of the paper is as follows. The electric drive analysed is described in section II, together with the experimental layout. Then, in section III, the frequency domain model is presented and validated from the FEM impedance of the machine. Furthermore, a step-by-step modelling approach of each component is presented in section IV, starting with the converter model, then proceeding to the cable, the electrical machine and finally the EMC filter. The drive's time domain model is validated with the voltage and current spectra. Finally, in section V, the main conclusions are outlined, and the future challenges for an effective EMC-orientated design are highlighted.

II. EXPERIMENTAL LAYOUT

The drive consists of the Permanent Magnet Synchronous Motor (PMSM), the power cable, the converter that generates the CMV and the filter that prevents the CM current from reaching the grid. The specification of the system are summarised in Table 1.

TABLE 1: Parameters of analysed system.

Pole pairs	Power	Grid Voltage	Torque	Current	Speed
15	4.5 kW	400 V	250 Nm	9 A	150 rpm

The experimental layout is shown in Fig. 1 (a), and the full drive schematic with the measurement points is shown in Fig. 1 (b). The system to be measured is on a wooden pallet to avoid parasitic couplings as far as possible.

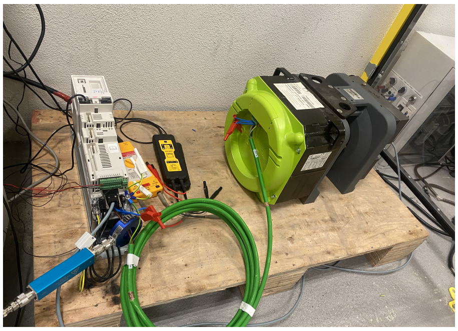

(a)

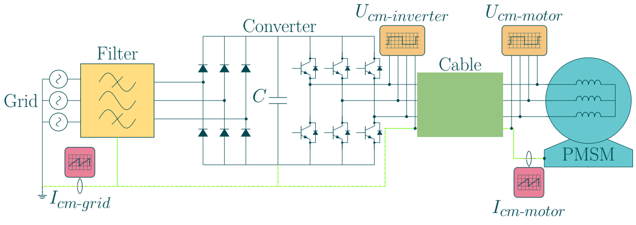

(b)

FIGURE 1: Analysed electrical drive. (a) Experimental Layout; (b) Schematic.

To validate the whole drive model, some measurements have been conducted and compared with the simulations. The CM voltage has been measured at the converter output and at the motor input to consider the effect of the power cable. The current has also been measured at the motor and at the grid connection point.

The voltage probes used for the measurement are PMK BumbleBee with a bandwidth of 400 MHz. The current has been measured with a TEKBOX TBCP2-750 RF current monitoring probe whose frequency measurement range is 1 kHz to 1 GHz and the transient limiter TBFL1 with a range of 9 kHz to 600 MHz. These signals have been read and saved with a RIGOL oscilloscope model MSO5204 of 200 MHz 4 channels and 8 GS/s.

Before comparing the simulations with the measurements, the accuracy of the experimental data must be carefully verified. In fact, when measuring high-frequency signals in the range of 150 kHz to 30 MHz, other devices can interfere with these measurements. Moreover, it must be taken into account that either the probes and the oscilloscope themselves might have some noise background.

To analyse this, the oscilloscope and the voltage and current probes have been placed in the measurement position, but with the drive switched off. Then, voltage and current have been measured and their spectra obtained, as shown in Fig. 2. This noise has been compared with all the next measurements to establish the limitations of each of them. The transfer impedance of the current probe is also included in the figure, as it is an important element to consider when measuring and post-processing the current measurements.

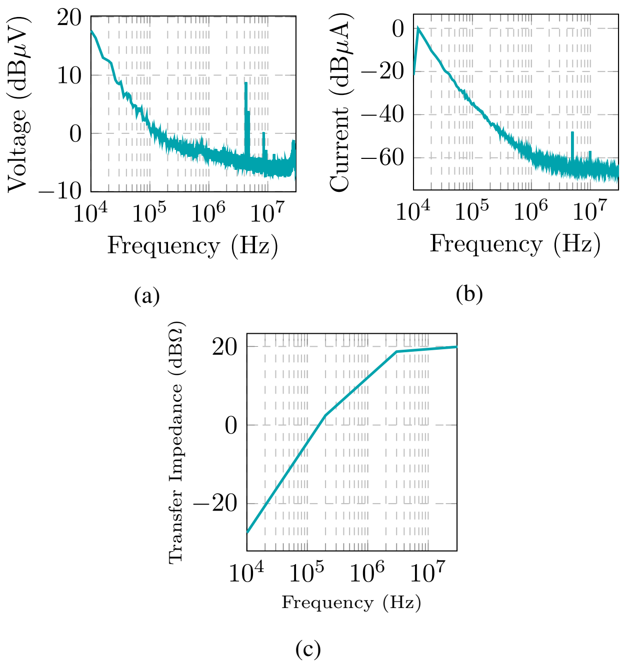

FIGURE 2: Probes: (a) Voltage probe Background noise; (b) Current probe Background noise. (c) Current probe transfer impedance

There are two domains for modelling electrical drives for EMI analysis, the frequency domain and the time domain. Although working in the frequency domain is more intuitive once the CM impedance of the motor is obtained with FEM simulations or measurements, the overvoltages and transient voltages at the motor terminals cannot be predicted in this domain. Therefore, the full drive model has been developed in the time domain. This approach allows for the observation of changes in the grid current and overvoltages at motor terminals.

III. FREQUENCY DOMAIN MACHINE MODEL

The electrical machine high-frequency impedance is obtained running FEM simulations with Altair Flux Software, as explained in [25]. For the validation of the impedance results, the common-mode and differential-mode impedances of 28 electrical machines, were measured in a factory manufacturing line.

All the motors were of the same model, and so 28 different motors were assessed to consider the effect of the manufacturing tolerance on the measured impedance. The common mode impedance is shown in Fig. 3, where the manufacturing tolerance is indicated by the green area between the maximum and minimum measured impedances. The tolerance was very low, suggesting that the impedance of all machines was almost equal, regardless of the manufacturing tolerance.

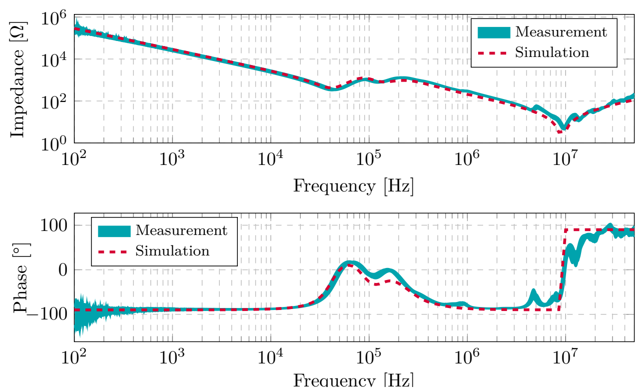

FIGURE 3: CM model of the machine. Experimental vs. FEM result. [25]

An inductive effect was observed around 10 MHz that depended on not only the measured device but also the measuring connections. Thus, an measurement was conducted with different calibrations of the impedance meter, revealing that the measuring connections introduced an inductance of approximately 3.75 μH to the measured impedance. Thus, this inductance is added in series to the simulated impedance to compensate for it.

Then, the rms error of the FEM impedance compared with the measured impedance is calculated as shown in eq. (1), where N refers to the number of frequency points.

$$\epsilon_{rms-FEM} = \sqrt{\frac{\sum_{\mathrm{f}=1}^{n} \left| \frac{\log(|Z_{\mathrm{Measured}}(f_i)|) - \log(|Z_{\mathrm{FEM}}(f_i)|)}{\log(|Z_{\mathrm{Measured}}(f_i)|)} \right|^2}{N}} \tag{1}$$

The resulting error of 6 %, is considered accurate for the prediction of the high-frequency impedance of the machine.

In order to validate the machine model in the frequency domain, Ohm's law has been used. To obtain the spectrum of the common-mode current, the spectrum of the voltage measured at the motor terminals is divided by the CM impedance of the machine simulated by FEM [25]. Then, this calculated current has been compared with the experimental measurement. The diagram is shown in Fig. 4 and the common-mode voltage spectrum measured in the motor is shown in Fig. 5.

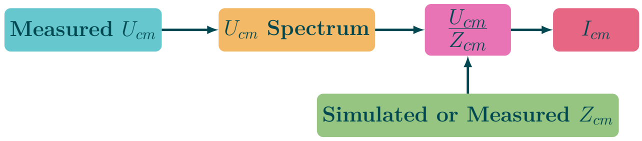

FIGURE 4: Validation process of the frequency-domain model of the electrical machines.

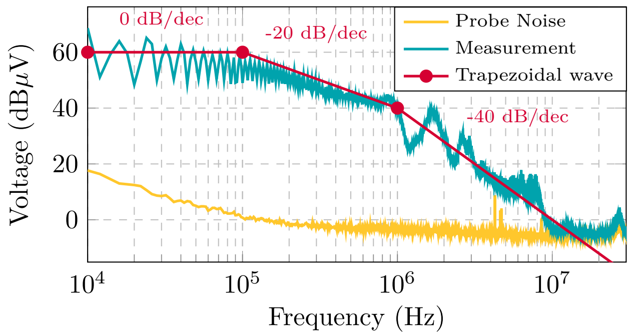

FIGURE 5: Motor Input common-mode voltage. Experimental measurement.

Given that above 10 MHz the measured voltage is below the noise background of the probe, the validity of the voltage measurement is compromised beyond this frequency. Consequently, the resulting current will be subject to comparison only up to the 10 MHz threshold.

The obtained current spectra are shown in Fig. 6. When the voltage is divided by the impedance obtained with the FEM simulation, the current spectrum shown in red is obtained. The yellow and dark blue currents are obtained by dividing the voltage by the maximum and minimum measured impedances of the 28 machines, respectively.

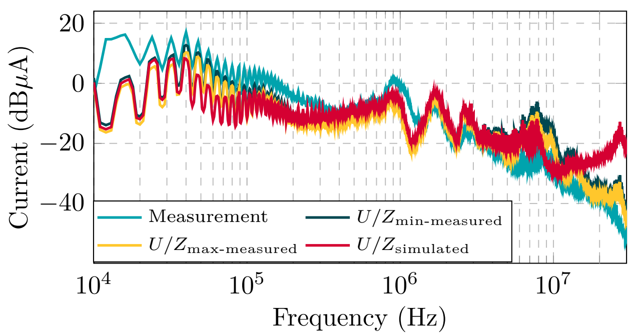

FIGURE 6: Frequency domain common-mode current. Experimental vs. Simulation results.

It can be seen that the currents obtained with the FEM impedance and the ones obtained using the measured impedances agree with each other. Furthermore, even if at some points there is a small discrepancy between the calculated and measured currents, there is overall agreement in the analysed frequency range with respect to resonance points and current value. Consequently, the current spectrum of the machine model has been validated in the frequency domain.

IV. TIME DOMAIN MODEL

Upon validation of the electric motor model in the frequency domain, attention is now turned to the development of the time domain model for the entire electric drive. This section is dedicated to the characterisation of the electric drive components, with the aim of incorporating all common-mode current paths present in the drive.

Subsequently, these components are integrated into a Matlab Simulink model. The model is then subjected to time-domain simulation to derive the common-mode voltage frequency spectrum. As mentioned above, the drive system under consideration is depicted in Fig. 1.

A. HIGH-FREQUENCY MODEL OF THE INVERTER

In the analysed drive, the grid feeds a converter. Initially, a three-phase diode rectifier feeds an uncontrolled DC bus containing a capacitor. Subsequently, a three-phase converter of IGBTs generates a PWM-modulated voltage according to the voltage and frequency requested by the drive control. These indications are those generated by the torque and speed required for the motor.

This converter is the root cause of conducted EMI, as it is the generator of the CM voltage coupled to its voltage pulses. However, the scope of this paper is focused on the electrical machine, so a behavioural model of the converter has been developed.

The behavioural model of the converter modulation is shown in Fig. 7. It produces modulated voltages through basic PWM generation by comparing a sinusoidal wave of the desired frequency with a triangular wave at a switching frequency of 8 kHz. The resulting rectangular pulse is modified to a trapezoidal one using a saturated integrator, in order to introduce rise and fall times in the switching pulses, as it is crucial for the common-mode voltage spectrum. The rise and fall times have been adjusted from the experimental characterisation of the converter.

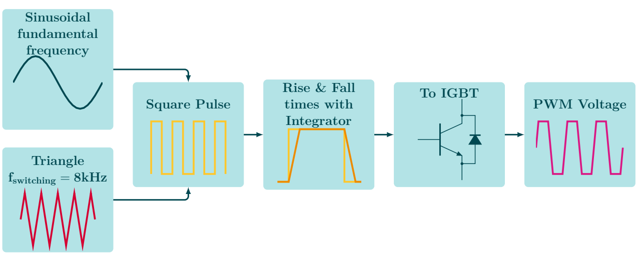

FIGURE 7: Converter modulation diagram.

Assuming the voltage is a trapezoidal wave with amplitude $V_{dc}/2$, duty cycle d, switching frequency f_s and rise and fall times t_r, the spectrum envelope in the frequency domain is:

This article has been accepted for publication in IEEE Access. This is the author's version which has not been fully edited and content may change prior to final publication. Citation information: DOI 10.1109/ACCESS.2024.3459641

$$|V_{\mathrm{CM}}(f)| \simeq \underbrace{V_{\mathrm{dc}} \cdot d}_{0\ \mathrm{dB/dec}} \cdot \underbrace{\left|\mathrm{Sinc}\left(\frac{\pi \cdot f \cdot d}{f_s}\right)\right|}_{-20\ \mathrm{dB/dec}} \cdot \underbrace{\left|\mathrm{Sinc}\left(\pi \cdot f \cdot t_r\right)\right|}_{-40\ \mathrm{dB/dec}} \tag{2}$$

where $\mathrm{Sinc}(x) \triangleq \sin(x)/(x)$ [13], [26]. As it can be concluded from the equation, and seen the red envelope in Fig. 4, the switching frequency changes the second asymptotic line, whereas the rise time defines the last part of the spectrum.

The model also includes the common-mode current paths shown in Fig. 8. In addition, the bus capacitance has been modelled as an RLC series branch to account for its high-frequency behaviour. Note that the impedances of the different phases of the input to ground and the output to ground are the same, as well as those of the positive and negative DC bus to ground.

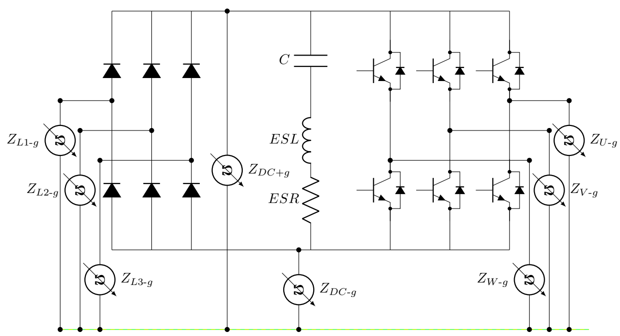

FIGURE 8: Converter CM current path characterisation.

CM impedances are simulated with RLC branches that match the measurements, as shown in Fig. 9. The RLC parameters to obtain these impedances are shown in Table 2.

TABLE 2: Parameters of the parasitic paths of the converter.

Path	R_{series} (Ω)	L_{series} (μH)	C_{series} (nF)
Z_{L1-g}	6.80	0.12	0.40
Z_{DC+-g}	2.04	0.13	0.50
Z_{U-g}	2.53	0.16	0.44

It must be remarked that the parasitic components of each IGBT have not been modelled for the behavioural model, only the impedances mentioned above and the switching procedure. These parasitic current paths should be enough to characterise the CM currents of the entire electric drive to conduct EMI analysis.

B. HIGH-FREQUENCY MODEL OF THE POWER CABLE

The modelling of the power cable is another key point in the drive, as it could considerably affect the common-mode voltage and current spectra at the motor terminals. The well-known PI model of an electric line has been used to model the cable, as shown in Fig. 10. In this case, 20 PI sections per phase have been used to make it more distributed, as described in [27].

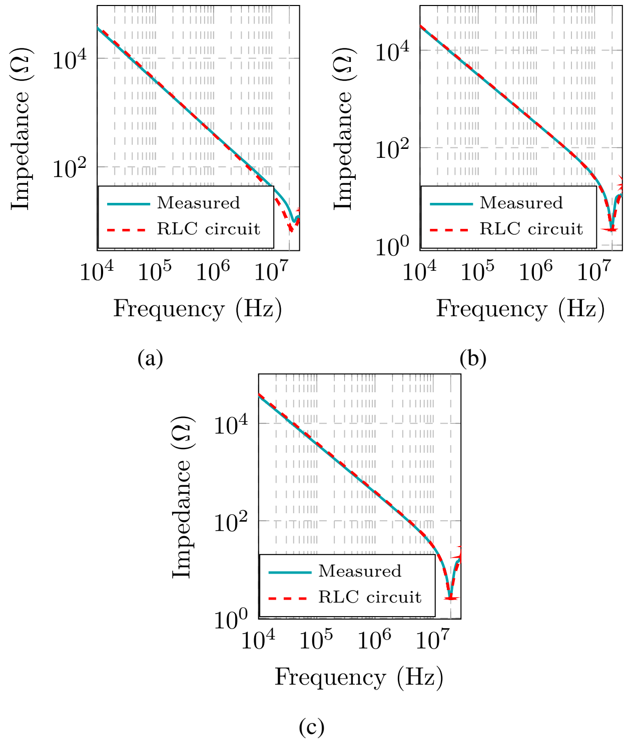

FIGURE 9: CM impedance of the converter. Experimental vs. Simulation results. (a) Z_{L1-g}; (b) Z_{DC+-g}; (c) Z_{U-g}.

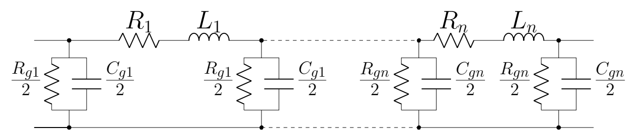

FIGURE 10: High-frequency PI model for the cable.

The power cable has been characterised using its differential mode and phase-to-ground impedances (Fig. 11), paying more attention to the latter, as the interest is focused on CM currents. The values of the distributed circuit parameters to obtain those impedances are shown in Table 3.

TABLE 3: Parameters of the PI model of the power cable per segment.

R_i	L_i	C_{gi}	R_{gi}
0.049 Ω	1.57 μH	20 pF	400 GΩ

The cable parameters have been adjusted numerically by comparing the model impedance with the measured one as the frequency dependency of R L parameters and the circuit distribution makes it complex to work with a analytical equation. However, the approximate relation of the model parameters with the impedances is shown in eq. (3). In fact, the R L parameters are related to the phase impedance, whereas the C_g and R_g are related to the CM impedance. These equations are valid until approximately 10 MHz, then both modes get coupled and the equations are no longer valid.

$$\begin{cases} Z_{phase}(f) & = R(f) + j2\pi f L(f) \\ Z_{phase-ground}(f) & = \frac{1}{2\pi f C_g} \end{cases} \quad (3)$$

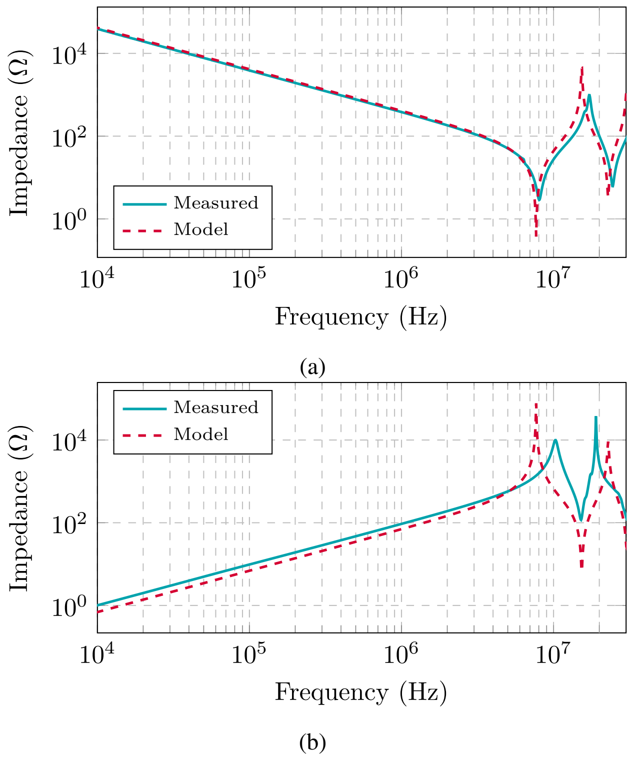

FIGURE 11: Impedance of the cable. Experimental vs. Simulation results: (a) Phase to ground; (b) Differential-mode.

C. TIME-DOMAIN MODEL OF THE ELECTRICAL MACHINE

In [25], a FEM simulation process had been described to obtain the machine's DM and CM impedances accurately. The software used for the FEM simulation is Altair Flux. However, these impedances are frequency dependent and must be modified to integrate them into the time-domain model of the overall electric drive. For this purpose, the lumped parameter circuit shown in Fig. 12 has been used as proposed in [27]. The impedance obtained from the FEM model in [25] has been used to define the circuit parameters so that the circuit impedance fits the impedance obtained by FEM.

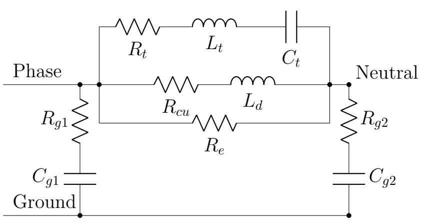

FIGURE 12: Machine's Time-Domain Equivalent Circuit.

The main impedance of the phase winding consists of R_{cu} and L_d, while R_t, L_t and C_t refer to the high-frequency effects on the winding. Then R_e accounts for the core losses. Finally, R_{g1}, C_{g1}, R_{g2}, and C_{g2} represent the parasitic couplings from the winding to the ground.

These circuit parameters must be defined to match the CM and DM impedances obtained from the FEM simulation explained in [25]. This can be done manually or using optimisation algorithms. In this case, the parameters have been adjusted using a global optimisation function consisting of a genetic algorithm. It must be remarked that priority has been given to the CM impedance, since the CM currents are the main objective of this work.

When adjusting the time domain model with the FEM impedance simulation, the impedance error has been defined as an objective to minimise. The per unit exponent error for each frequency point has been calculated as shown in eq. (4), where $Z_{\text{FEM}}(f_i)$ is the FEM impedance value for the i^{th} frequency and $Z_{\text{model}}(f_i)$ is the impedance value of the model to adjust.

$$\Delta(f_i) = \left| \frac{\log(|Z_{\text{FEM}}(f_i)|) - \log(|Z_{\text{model}}(f_i)|)}{\log(|Z_{\text{FEM}}(f_i)|)} \right| \quad (4)$$

Then, the root mean square error for each defined frequency range is obtained in equation eq. (5). The number of points for the rms value is defined as N and refers to the points of the frequency range.

$$error_{rms} = \sqrt{\frac{\sum_{\text{f}=1}^{n} \Delta(f_i)^2}{N}} \quad (5)$$

Six different error objectives have been defined to catch all resonances. The error resulting from the optimisation of the genetic algorithm in each frequency range is shown in Table 4.

TABLE 4: Error of the time domain model of the motor respect to the FEM impedance.

Mode	< 20 kHz	20 kHz – 300 kHz	> 300 kHz
DM	2.77 %	3.88 %	1.09 %
CM	0.22 %	0.91 %	0.96 %

The low frequency impedance has been adjusted to consider the nominal conditions of the drive, which, in fact, will define the nominal current of the drive. The intermediate frequency range has been then analysed for the resonances in CM and DM modes, and the high frequency range has been used for the last part of the impedance after the resonance.

Furthermore, it is interesting to see how the different parameters converge during the algorithm to minimise the resulting error in the impedance. For instance, as shown in Fig. 13, C_{g1} is important in the high frequency range, while C_{g2} is crucial in the lower frequency range.

The resulting impedances are shown in Fig. 14, which shows no error in the CM impedance and a small error in the resonance point of the DM impedance, as expected.

The circuit parameters obtained from the genetic algorithm to obtain the impedances in Fig. 14 are shown in Table 5.

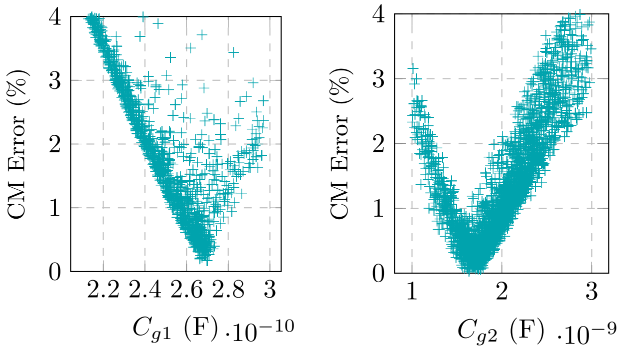

FIGURE 13: Circuit parameter convergence: (a) C_{g1} (300kHz<f<30MHz); (b) C_{g2} (f<20kHz)

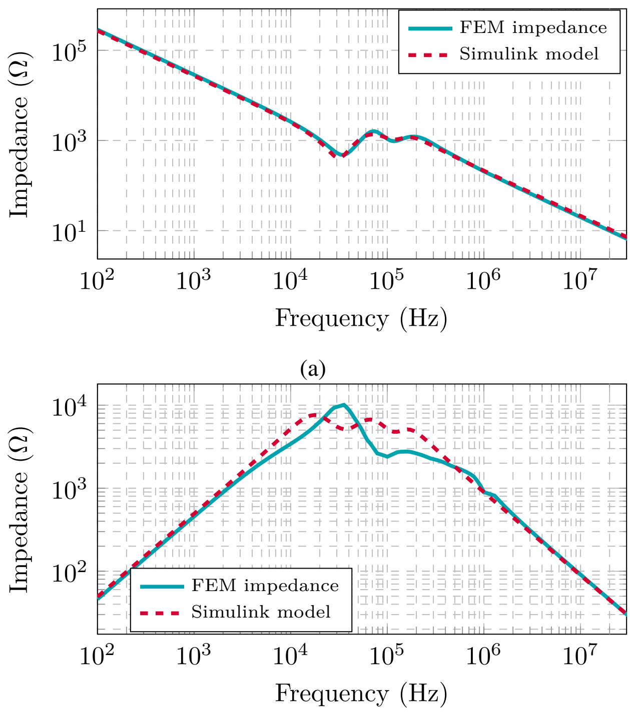

FIGURE 14: Impedance of the motor. FEM model from [25] vs simulation results. (a) CM; (b) DM.

TABLE 5: Calculated values for the parameters of the electrical equivalent circuit of the PMSM

Parameter	Value	Parameter	Value
R_{g1}	5 Ω	R_t	1 kΩ
C_{g1}	0.1 nF	C_t	0.1 nF
R_{g2}	0.1 Ω	L_t	18.5 mH
C_{g2}	0.85 nF	R_{Cu}	1.33 Ω
R_e	5 $k\Omega$	L_d	7.6 mH

D. FILTER

Once the drive components are designed, it is necessary to verify compliance with the EMC standards specified by EN-12015 [22]. Even if the current has been measured with a current RF probe, the regulations are defined by the emissions in dBμV, because they are usually measured by Line Impedance Stabilisation Networks (LISN). Therefore, to convert dBμA to dBμV a constant impedance of 50 Ω has been used in all frequency ranges, as it is the standard impedance for RF measurements. As can be seen in Fig. 15, the current exceeds the regulations at the connection point of the grid, which can interfere with other elements connected to the grid.

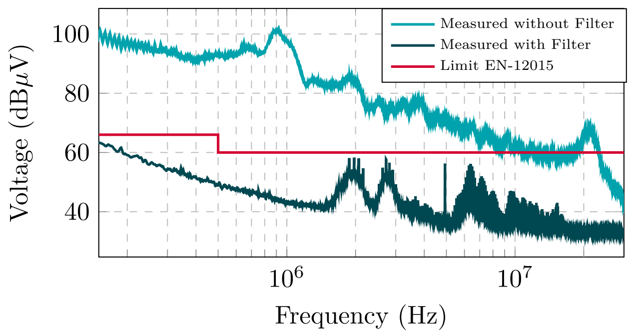

FIGURE 15: Grid current with and without EMC filter. Experimental measurements.

To solve this problem and comply with the regulations, the filter shown in Fig. 16 has been introduced between the converter and the grid, filtering the current emission to the grid as shown in Fig. 17. These attenuation data are obtained by measuring the S21 parameter with a vector network analyser, representing the transfer function V_{in}/V_{out} where V_{in} is the input voltage of the filter and V_{out} is the output voltage.

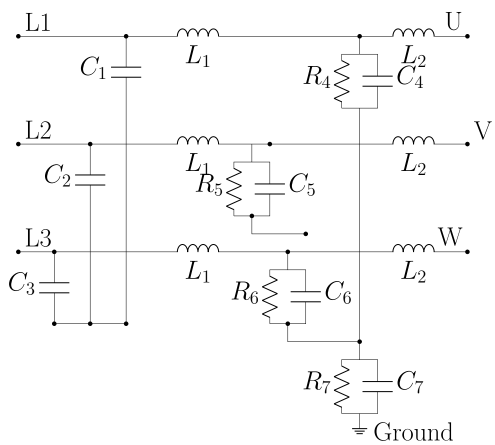

FIGURE 16: Electric circuit of the EMC filter.

The filter electric parameters are shown in Table 6. As mentioned before, this adds a new component, weight, volume, and cost to the electric drive but does not solve the root problem; it just mitigates the consequences.

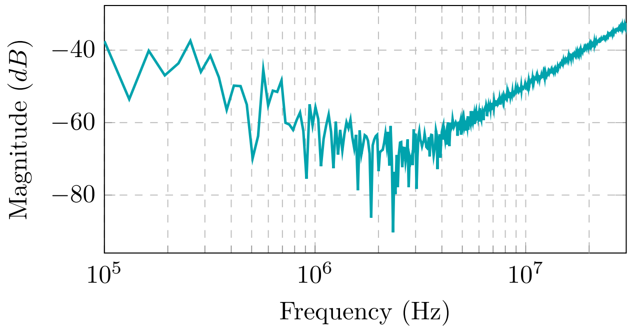

FIGURE 17: Attenuation of the EMC filter.

TABLE 6: Filter parameters.

Parameter	Value	Parameter	Value
L_1	6.3 mH	L_2	10 μH
$C_{1\text{-}6}$	2.85 μF	C_7	5.7 μF
$R_{4\text{-}6}$	200 Ω	R_7	680 Ω

The model has been calibrated with impedance measurements of a between input terminals (L_{1-2-3}) and output terminals (U-V-W), phase-to-ground in the input, and phase-to-ground in the output, as has been done with the converter previously. The resulting impedances are shown in Fig. 18.

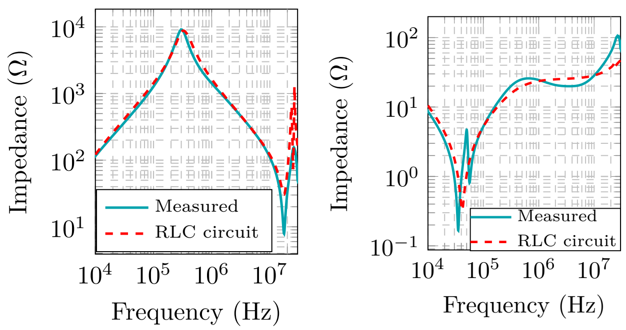

(a) (b)

FIGURE 18: Filter impedance. Experimental vs. Simulation results: (a) Z_{L2-g}; (b) Z_{U-g}.

Using eq. (1) the rms error of both impedances Z_{L2-g} and Z_{U-g} is calculated for the EMC range, being respectively 1.9 % and 5.8 %. Thus the model of the filter is accurate for the desired aim of analysing EMI of the drive.

E. VALIDATION

1) Validation of the Motor Model

Initially, the measured CM voltage at the motor terminals (Fig. 5) has been introduced to the motor model to compare the measured CM current with the simulated one. In Fig. 19, the layout of the simulation is shown.

As expected, the accuracy of the machines's time domain model is acceptable, as it can be seen in the current spectrum shown in Fig. 20. Therefore, the accuracy of the time domain model of the machine is ensured, for further analysis of the full drive.

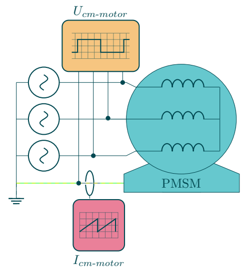

FIGURE 19: Motor's time domain model layout diagram.

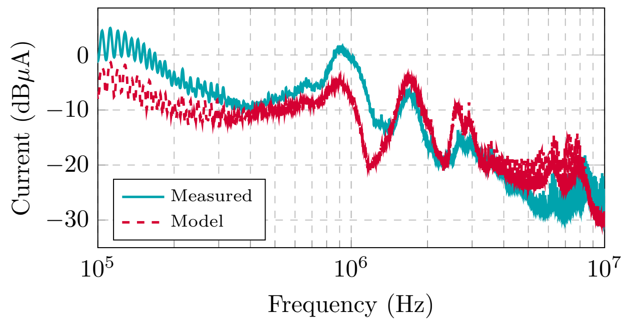

FIGURE 20: Electrical motor CM current. Experimental vs. Simulation results.

2) Validation of the Full Drive Model

Upon the independent examination of the machine, the whole drive system undergoes a process of validation. This involves measuring the CM voltage at both the converter output and the motor input, which serves to verify the amplification attributed to the power cable. In addition, the CM current has been measured at three different points: the motor input, the converter output, and the grid connection point. The measurement layout is depicted in Fig. 21.

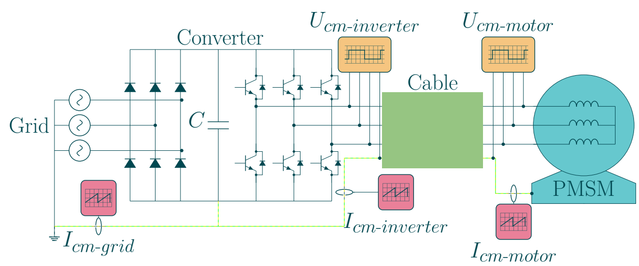

FIGURE 21: Full drive time domain model layout.

The grid supplies a three-phase 400 V system with protection or ground conductor. Then this voltage is rectified by an uncontrolled diode rectifier that generates a 560 V DC bus. Then, using modulation techniques as explained in section IV-A, the machine is set to its nominal speed without load, resulting in the CM voltage spectrum plotted in Fig. 22. It agrees with the measured voltage.

It can be seen that the model agrees accurately, except for some minimal resonances in the range of 800 kHz–1 MHz and around 2 MHz. As can be seen, the overall voltage spectrum pattern agrees with the measurement, so the modulation patter

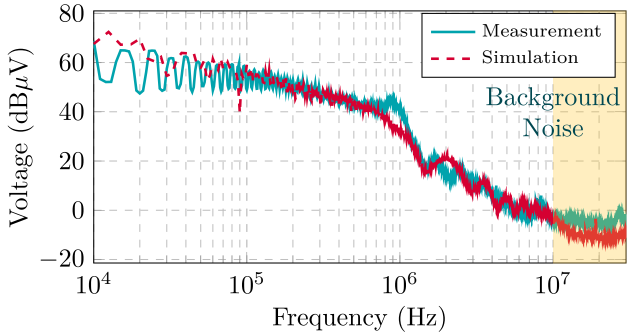

FIGURE 22: Common mode voltage at converter output. Experimental vs. Simulation results.

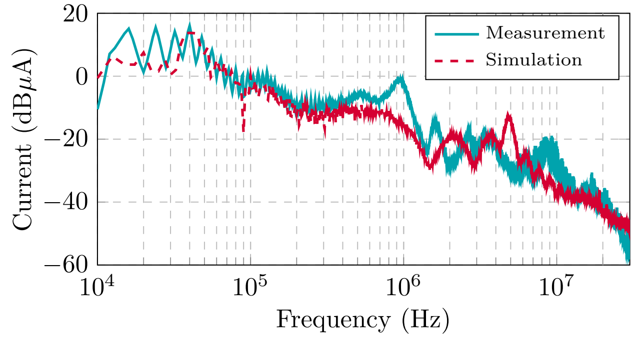

FIGURE 24: Motor input CM current. Experimental vs. Simulation results.

is properly simulated. Thus, the mismatch in these points may be derived from the parasitics of the converter.

As expected, the voltage from 10 to 30 MHz is lower than the measured one, due to the probe background noise mentioned in the above sections. However, it must be remarked that the current probe measurements are valid in the full EMC frequency range, as their background noise is lower than the measurements.

In Fig. 23, the CM voltage at the motor terminals is depicted. The overall tendency agrees with the measurement, even if the resonances at 1.5 and 3 MHz are slightly displaced. These are the amplification of the slight differences in the CM voltage in the output of the converter due to the effect of the cable. Moreover, the small peak at 5 MHz may be due to the slight underestimation of the impedance at the resonance point of the CM impedance model of the cable. It should also be noted that the voltage level is higher than in the converter output because of the amplification introduced by the power cable.

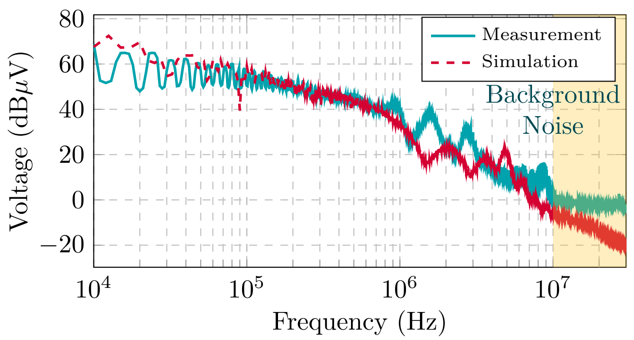

FIGURE 23: Motor input CM voltage. Experimental vs. Simulation results.

Then, in Fig. 24 the CM current of the motor is presented. Overall, the simulation agrees with the measurement except for resonances from 1 to 5 MHz that had already been displaced in the CM voltage analysed at motor terminals. Apparently, this may be due to small inaccuracies in the converter and cable model because the motor model has been previously precisely validated in Fig. 20.

Finally, the current in the grid connection point is validated in Fig. 25. As before, the overall spectrum agrees with the measurement, despite the small resonances previously missing in the motor input voltage, which are also missing in the final grid current. Moreover, the resonance at 20 MHz caused by the power cable parasitics is represented by the model, even if a bit overestimated. This higher peak value is due to the input to ground impedance (Z_{L1-g}) difference at that frequency point.

It should be noted that the converter model considers the parasitic impedances shown in Fig. 8, but the inner parasitics of each IGBT are not modelled, as it is not within the scope of the present work.

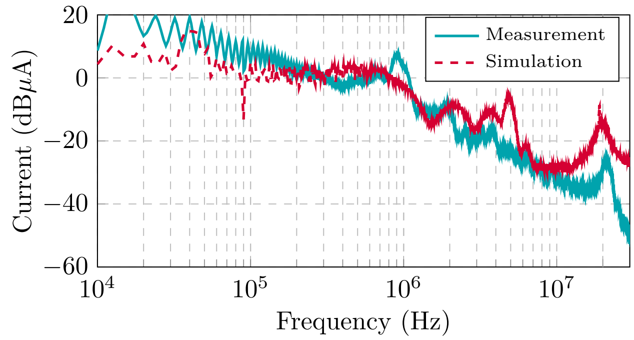

FIGURE 25: Grid input CM current. Experimental vs. Simulation results.

This section showed that the full drive model agrees with the overall measurement spectrum. In the next section, further analysis is made with the presented model in order to reduce the CM current conducted to the grid.

Interestingly, by analysing the CM current at the different points as shown in Fig. 21, the influence of each drive component can be appreciated. In Fig. 26, the different currents are compared. It can be seen that the output currents of the grid and the converter are higher than the one at the motor input. This is due to parasitics in the power cable and the converter, which also generate current paths to the ground. For example, from 100 kHz to 2 MHz it looks like the mayor parasitic current flows from the power cable to ground due to the gap

This article has been accepted for publication in IEEE Access. This is the author's version which has not been fully edited and content may change prior to final publication. Citation information: DOI 10.1109/ACCESS.2024.3459641

between the motor and the converter output current. The peak around 20 MHz is interesting because it is not present in the motor current but it is present in the converter output and the grid, so it may be derived from the power cable's parasitic paths.

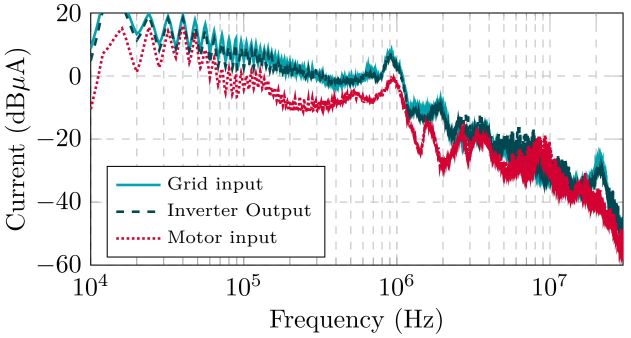

FIGURE 26: Measured CM current in different measuring points.

3) Validation of the Full Drive Model with filter

In Fig. 27, the CM current for the motor is depicted using the filtered drive model. Generally, the simulation results are consistent with the actual measurements, with the exception of some small resonances occurring between 1.5 to 5 MHz, which are also observed in the CM current at the motor's input in the unfiltered model.

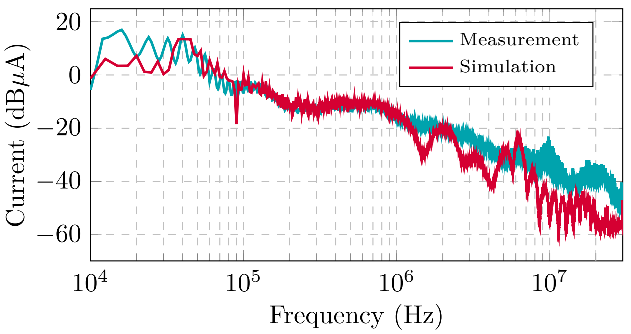

FIGURE 27: Common mode currents on the Motor. Experimental vs. Simulation Results.

In Fig. 28 the CM current delivered to the grid is plotted. Similarly to earlier observations, the complete spectrum is consistent with the measurements, although it lacks the minor resonances that are absent in the motor input voltage and are not observed in the final grid current either. It should be noted that the difference between the measurement and the simulation from 10 to 150 kHz is due to the background noise of the current probe, as mentioned in Fig. 2b. In any case, it is important to emphasise that this frequency range, as it is below 150 kHz, is outside the frequency range defined by standards for conducted EMI.

Finally, the current in the input of the grid is illustrated in dBμV to check the standard limit of EMC emission. The simulation with a filter is compared to the one without it

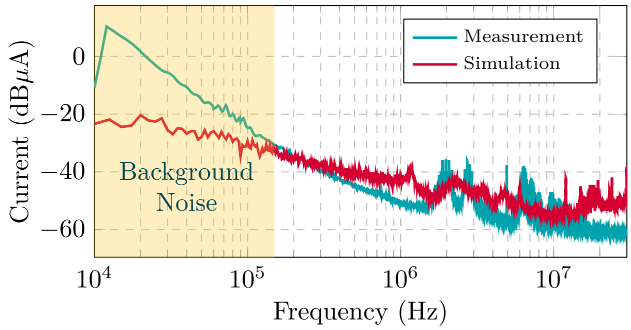

FIGURE 28: Grid input CM current with filter. Experimental vs. Simulation Results.

in Fig. 29. It can be seen that the current without filter is outside the standard, which replicates the result reported by the experimental measurements.

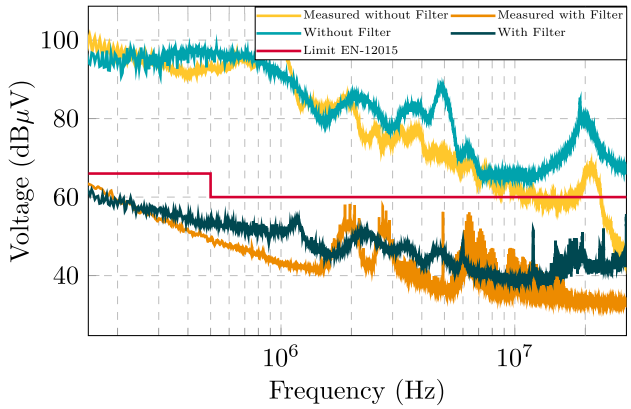

FIGURE 29: Grid input CM current comparison with or without EMC filter. Measurement vs. Simulation results.

V. CONCLUSIONS

In the literature, the analysis of a full electric drive typically involves the use of machine models that are lumped parameter networks. These models rely on parameters fitted from experimental measurements, not allowing for predictive capabilities during the design stage of the machine.

In contrast, this study experimentally validates a full-drive model utilising motor impedance data derived from FEM simulations. This data has been fitted to a lumped-parameter model via a basic genetic algorithm, demonstrating a significant agreement with experimental data.

The inverter and cable models employed are based on impedance measurements, despite the primary focus of the research is the electric motor. Nevertheless, the accuracy achieved for the full simulation is deemed sufficient.

The developed full-drive model is beneficial for examining the high-frequency behaviour of the overall system as the motor's impedance changes. This highlights its crucial role in the design process of electric drives. The model indicates that motor impedance influences the full drive common-mode current, albeit within certain frequency ranges. In the anal-

This article has been accepted for publication in IEEE Access. This is the author's version which has not been fully edited and content may change prior to final publication. Citation information: DOI 10.1109/ACCESS.2024.3459641

ysed case, this has been observed from 150 kHz to 3 MHz. Beyond 3 MHz, the significance transitions to the inverter and cable pathways.

Finally, the filter used for the EMC standard compliance is also incorporated and validated within the model, culminating in a complete drive simulation. This achievement facilitates a more accurate simulation of the full drive.

Further research from the authors will focus on the optimisation of the high-frequency CM impedance of electrical machines. Design parameters that could be modified to decrease drive CM currents are currently being identified. Additionally, validating the model for a WBG based converter will complete the model for their use, and using a LISN for the measurement would complete the experimental procedure.

REFERENCES

[1] United Nations, "Sustainable development goals," 2015, accessed: 12/01/2024. [Online]. Available: https://sdgs.un.org/goals

[2] European Parliament, "More electric cars on EU roads by 2030," 2018. [Online]. Available: https://www.europarl.europa.eu/news/en/press-room/20180911IPR13114/more-electric-cars-on-eu-roads-by-2030

[3] International Energy Agency, "Key World Energy Statistics," IEA, Tech. Rep., 2021. [Online]. Available: https://www.iea.org/reports/key-world-energy-statistics-2021

[4] A. K. Morya, M. C. Gardner, B. Anvari, L. Liu, A. G. Yepes, J. Doval-Gandoy, and H. A. Toliyat, "Wide Bandgap Devices in AC Electric Drives: Opportunities and Challenges," *IEEE Transactions on Transportation Electrification*, vol. 5, no. 1, pp. 3–20, 3 2019. [Online]. Available: https://ieeexplore.ieee.org/document/8611115/

[5] B. Zhang and S. Wang, "A Survey of EMI Research in Power Electronics Systems with Wide-Bandgap Semiconductor Devices," *IEEE Journal of Emerging and Selected Topics in Power Electronics*, vol. 8, no. 1, pp. 626–643, 2020.

[6] P. Mazurck, A. Michalski, H. Swiatck, C. Mazzetti, and Z. Flisowski, "Hazard for insulation and relevant emc problems due to voltages in circuits of motor supply by pwm converters," in *2003 IEEE Bologna Power Tech Conference Proceedings,*, vol. 2. IEEE, 2003, pp. 728–732. [Online]. Available: http://ieeexplore.ieee.org/document/1304637/

[7] Z. Shen, D. Jiang, T. Zou, and R. Qu, "Dual-Segment Three-Phase PMSM With Dual Inverters for Leakage Current and Common-Mode EMI Reduction," *IEEE Transactions on Power Electronics*, vol. 34, no. 6, pp. 5606–5619, 6 2019. [Online]. Available: https://ieeexplore.ieee.org/document/8440757/

[8] G. Spadacini, F. Grassi, and S. A. Pignari, "Conducted emissions in the powertrain of electric vehicles," in *2017 IEEE International Symposium on Electromagnetic Compatibility & Signal/Power Integrity (EMCSI)*, vol. 69, no. July. IEEE, 8 2017, pp. 1–28. [Online]. Available: http://ieeexplore.ieee.org/document/8078064/

[9] E. Robles, M. Fernandez, E. Ibarra, J. Andreu, and I. Kortabarria, "Mitigation of common mode voltage issues in electric vehicle drive systems by means of an alternative AC-decoupling power converter topology," *Energies*, vol. 12, no. 17, p. 3349, 8 2019. [Online]. Available: https://www.mdpi.com/1996-1073/12/17/3349

[10] K. Vostrov, J. Pyrhonen, M. Niemela, J. Ahola, and P. Lindh, "Mitigating Noncirculating Bearing Currents by a Correct Stator Magnetic Circuit and Winding Design," *IEEE Transactions on Industrial Electronics*, vol. 68, no. 5, pp. 3805–3812, 5 2021. [Online]. Available: https://ieeexplore.ieee.org/document/9057574/

[11] J. Zhang, M. Shen, and X. Zhao, "Study on the Effect of Inverter Modulation Methods and Operating Condition on Common Mode EMI for Motor Drive System," in *SAE Technical Papers*, vol. 2017-March, no. March, 3 2017. [Online]. Available: https://www.sae.org/content/2017-01-1223/

[12] E. Robles, M. Fernandez, J. Andreu, E. Ibarra, and U. Ugalde, "Advanced power inverter topologies and modulation techniques for common-mode voltage elimination in electric motor drive systems," *Renewable and Sustainable Energy Reviews*, vol. 140, no. January, p. 110746, 4 2021. [Online]. Available: https://doi.org/10.1016/j.rser.2021.110746https://linkinghub.elsevier.com/retrieve/pii/S136403212100040X

[13] G. Almeida, M. Cousineau, N. Rouger, S. Serpaud, V. D. Santos, B. Cougo, D. Guedon, O. Crepel, and R. Perraud, "Early-stage HF-EMC Simulation Analyses of Common-Mode Current in SiC-Based Motor Drive System for Modern Aircraft Applications," *IEEE Transactions on Transportation Electrification*, vol. 10, no. 2, pp. 4393–4406, 2023.

[14] T. Weber, "EMC filters in high voltage traction drive systems," *IEEE International Symposium on Electromagnetic Compatibility*, 2008.

[15] G. Vidmar and D. Miljavec, "A Universal High-Frequency Three-Phase Electric-Motor Model Suitable for the Delta- and Star-Winding Connections," *IEEE Transactions on Power Electronics*, vol. 30, no. 8, pp. 4365–4376, 2015.

[16] M. Schinkel, S. Weber, S. Guttowski, W. John, and H. Reichl, "Efficient HF Modeling and Model Parameterization of Induction Machines for Time and Frequency Domain Simulations," in *Twenty-First Annual IEEE Applied Power Electronics Conference and Exposition, 2006. APEC '06.*, vol. 2006. IEEE, 2006, pp. 1181–1186. [Online]. Available: http://ieeexplore.ieee.org/document/1620689/

[17] F. Zare, "Practical approach to model electric motors for electromagnetic interference and shaft voltage analysis," *IET Electric Power Applications*, vol. 4, no. 9, pp. 727–738, 2010.

[18] M. Cai, T. Craddock, and O. Wasynczuk, "High-frequency modeling, parameterization, and simulation of IPM motor drive systems," in *2017 IEEE Power and Energy Conference at Illinois (PECI)*. IEEE, 2 2017, pp. 1–8. [Online]. Available: http://ieeexplore.ieee.org/document/7935769/

[19] M. Mohammadi-Rostam, M. Shahabi, and A. A. Shayegani-Akmal, "High frequency lumped parameter model for EMI problems and over voltage analysis of Induction motor," *Journal of Electrical Engineering*, vol. 13, no. 3, pp. 278–283, 2013.

[20] H. Peng, N. Driendl, S. Stevic, D. Butterweck, Y. Firouz, L. Sharifian, and K. Hameyer, "High-frequency Modeling of Permanent Magnet Synchronous Machines using Grey Box Models," *IEEE Transactions on Transportation Electrification*, vol. PP, no. 8, pp. 1–1, 2024. [Online]. Available: https://ieeexplore.ieee.org/document/10423906/

[21] J. Sun and L. Xing, "Parameterization of Three-Phase Electric Machine Models for EMI Simulation," *IEEE Transactions on Power Electronics*, vol. 29, no. 1, pp. 36–41, 1 2014. [Online]. Available: http://ieeexplore.ieee.org/document/6519273/

[22] European Committee for Standardization, "EN 12015: Electromagnetic compatibility. Product family standard for lifts, escalators and moving walks. Emission." 2021. [Online]. Available: https://tienda.aenor.com/norma-une-en-12015-2021-n0065539

[23] Y. Kwack, H. Kim, C. Song, M. Moon, D.-H. Kim, B. Kim, E. Kim, and J. Kim, "EMI modeling method of interior permanent magnet synchronous motor for hybrid electric vehicle drive system considering parasitic and dynamic parameters," in *2015 Asia-Pacific Symposium on Electromagnetic Compatibility (APEMC)*. IEEE, 5 2015, pp. 78–81. [Online]. Available: http://ieeexplore.ieee.org/document/7175390/

[24] Y. Moreno, G. Almandoz, A. Egea, B. Arribas, and A. Urdangarin, "Analysis of Permanent Magnet Motors in High Frequency—A Review," *Applied Sciences*, vol. 11, no. 14, p. 6334, 7 2021. [Online]. Available: https://www.mdpi.com/2076-3417/11/14/6334

[25] Y. Moreno, A. Egea, G. Almandoz, G. Ugalde, A. Urdangarin, and R. Moreno, "High-Frequency Modelling of Electrical Machines for EMC Analysis," *Electronics*, vol. 13, no. 4, p. 787, 2 2024. [Online]. Available: https://www.mdpi.com/2079-9292/13/4/787

[26] F. Costa and D. Magnon, "Graphical analysis of the spectra of EMI sources in power electronics," *IEEE Transactions on Power Electronics*, vol. 20, no. 6, pp. 1491–1498, 2005.

[27] G. Almandoz, S. Zarate, A. Egea, Y. Moreno, A. Urdangarin, and R. Moreno, "High Frequency Modeling of Electric Drives for Electromagnetic Compatibility Analysis," in *2020 International Conference on Electrical Machines (ICEM)*. IEEE, 8 2020, pp. 1129–1135. [Online]. Available: https://ieeexplore.ieee.org/document/9270804/

YERAI MORENO was born in Irún, Spain, in 1996. He received his B.Sc. degree in electrical engineering from the University of the Basque Country, Spain, in 2018 and his M.S. degree in industrial engineering from Mondragon Unibertstitatea, Spain, in 2020. Since 2018, he has been with the Electronics and Computing Department, Mondragon Unibertsitatea, where he is currently pursuing his PhD. His current research interests include electrical machine design and EMC optimisation of electrical drives.

GAIZKA ALMANDOZ (M'04) was born in Arantza, Spain. He received the B.Sc. and PhD degrees in electrical engineering from Mondragon Unibertsitatea, Mondragón, Spain, in 2003 and 2008, respectively. Since 2003, he has been with the Electronics and Computing Department, Mondragon Unibertsitatea, where he is currently an Associate Professor. His current research interests include electrical machine design, modelling, and control. He has participated in various research projects in the fields of electric energy generation and electric traction systems.

ARITZ EGEA received the degree in electrical engineering from the University of Mondragon, Mondragón, Spain, in 2009, and the PhD degree in electrical engineering in 2012. He is currently an Associate Professor at the Faculty of Engineering, Mondragon Unibertsitatea. His current research interests include electrical machine design and control and electromagnetic actuators.

IMANOL EGUREN was born in Anoeta, Basque Country, Spain, in 1993. He received a B.S. degree in electronics engineering and the Ph.D. degree in applied engineering from Mondragon Unibertsitatea, Mondragón, Spain, in 2015 and in 2022, respectively. He is now a researcher and lecturer for Mondragon Unibertsitatea. His current research interests include design, control, and optimisation of electrical machines.

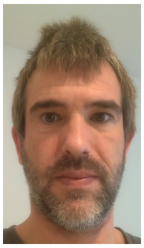

ANDER URDANGARIN was born in Ordizia. Spain, in February 1982. He received his B.Sc. degree in Automatic and Industrial Electronics from Mondragon Unibertsitatea, Mondragón, Spain, in 2009. Between 2010 and 2012, he was with the Department of Electronics of Mondragon Unibertsitatea. Since 2012, he has been a member of ORONA. His current research interests include power electronics design, modelling, and control.